Neuron
NeuroResource

Photoactivatable Neuropeptides for Spatiotemporally Precise Delivery of Opioids in Neural Tissue

Matthew R. Banghart[1] and Bernardo L. Sabatini[1,*]
[1]Department of Neurobiology, Howard Hughes Medical Institute, Harvard Medical School, Boston, MA 02115, USA
*Correspondence: bsabatini@hms.harvard.edu
DOI 10.1016/j.neuron.2011.11.016

SUMMARY

Neuropeptides activate G protein-coupled receptors to acutely modulate cellular excitability and synaptic transmission. However, due to the lack of reagents for precise delivery of peptides within dense brain tissue, the spatiotemporal scale over which neuropeptides act is unknown. To achieve rapid and spatially delimited delivery of neuropeptides in mammalian brain tissue, we developed photoactivatable analogs of two opioids: [Leu^5]-enkephalin (LE) and the 8 amino acid form of Dynorphin A (Dyn-8). These peptides are functionally inactive prior to photolysis, and exposure to ultraviolet (UV) light causes clean release of LE and Dyn-8. Recordings from acute slices of rat locus coeruleus (LC) demonstrated that photorelease of LE activates mu opioid receptor-coupled K^+ channels with kinetics that approach the limits imposed by G protein-mediated signaling. Temporally precise and spatially delimited photorelease revealed the kinetics and ionic nature of the mu opioid response and the mechanisms that determine the spatial profile of enkephalinergic volume transmission in LC.

INTRODUCTION

Neuropeptides are expressed and secreted throughout the mammalian brain, typically in combination with a fast neurotransmitter such as glutamate or GABA (Hökfelt et al., 2000). Neuropeptides are packaged in vesicles and several are known to be released in an activity-dependent manner (Ludwig and Leng, 2006). Neuropeptide expression is often regulated by neuronal activity and many neurons are classified by their selective expression of different neuropeptides and neuropeptide receptors (Hökfelt et al., 2000). Such regulated and heterogeneous expression of neuropeptides suggests a precise function in neuron-to-neuron signaling. Indeed, many aspects of synapse and cell function are modulated by neuropeptide-dependent activation of G protein-coupled receptors (GPCRs) (Strand, 1999; Tallent, 2008). At the behavioral level, neuropeptides have profound and complex neuromodulatory effects on brain function: they regulate social bonding (Insel, 2010), feeding (Morton et al., 2006), sleep (Adamantidis et al., 2010), aversion (Knoll and Carlezon, 2010), and reward (Le Merrer et al., 2009).

Studies into neuropeptide systems have been limited by a paucity of experimental tools. The conditions that trigger neuropeptide release from neurons are largely unknown and currently available methods of activating neuropeptide receptors in brain tissue prevent quantitative studies of their function. Although small-molecule agonists for many neuropeptide receptors are available, many GPCRs exhibit functional selectivity such that they are incompletely or unnaturally activated by synthetic ligands (Urban et al., 2007). Furthermore, neuropeptides can bind and activate multiple receptor subtypes present on the same cell with similar affinities (Lupica et al., 1992; Svoboda et al., 1999). Thus, exogenous application of peptide ligands, rather than synthetic agonists, more accurately mimics endogenous peptidergic signaling. However, compared to traditional pharmacological agents, peptides are large, hydrophobic molecules and thus diffuse slowly within the brain. Direct peptide application in vivo and in brain slices by perfusion, pressure injection (Williams et al., 1982), or iontophoresis (Travagli et al., 1995) produces a slowly rising, prolonged, and spatially imprecise presentation of the peptide. These methods offer poor control over the concentration of peptide delivered, largely limiting quantitative analysis to the effects of saturating doses for consistency (Duggan and North, 1983). However, such doses can rapidly trigger receptor desensitization and internalization, which limits robustness and experimental throughput. Therefore, typical peptide delivery methods can only reveal slow and spatially imprecise neuropeptide actions, leaving the possibility of short-lived, local neuropeptide signaling unexplored.

In dissociated neurons, peptide signaling reaches full activation within several seconds of agonist exposure and deactivates within seconds of washout (Ingram et al., 1997). However, in intact brain tissue, neuropeptide receptors are often found up to hundreds of microns from peptide release sites (Khachaturian et al., 1985), suggesting that neuropeptides are capable of volume transmission. Indeed, there is strong evidence that this phenomenon occurs in the spinal cord (Duggan, 2000). The spatiotemporal extent of neuropeptide signaling is determined by the poorly understood interactions of rapid GPCR signaling downstream of ligand binding, slow peptide diffusion, and the action of extracellular peptidases,

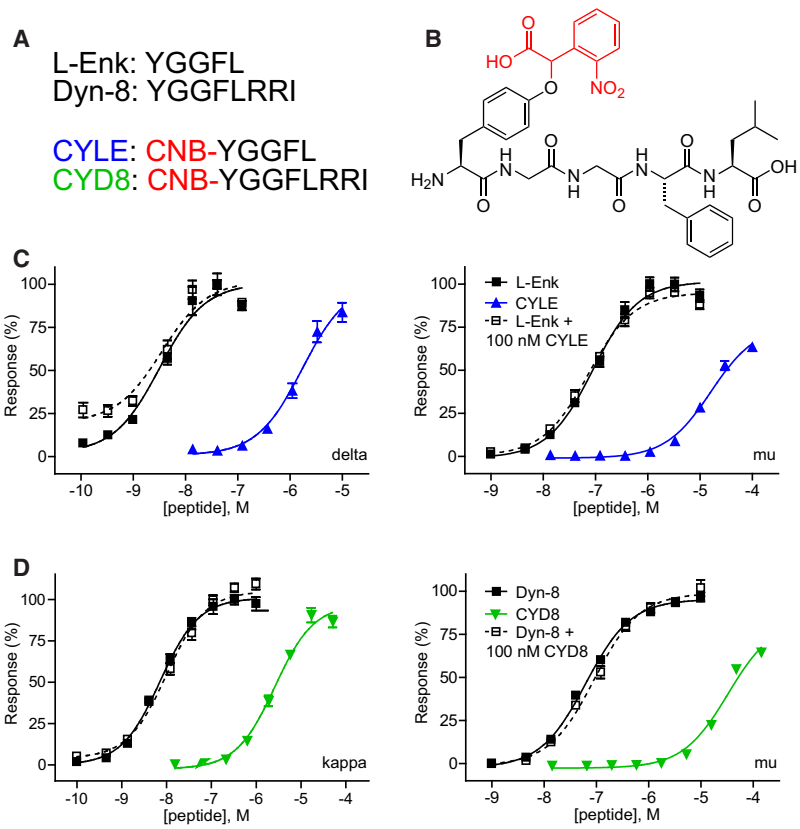

Figure 1. CYLE and CYD8 Are Caged LE and Dyn-8 Analogs, Respectively

(A) One-letter-code amino acid sequences of LE, Dyn-8, and the CNB-modified analogs CYLE and CYD8.

(B) Chemical structure of CYLE. The CNB moiety is drawn in red.

(C) Dose-response curves for LE (black squares), CYLE (blue triangles), and LE in 100 nM CYLE (open squares) at delta (left) and mu (right) opioid receptors. The solid lines depict the best-fit sigmoidal functions used to derive the EC_{50} values reported in the text. The dashed lines are fits to the data obtained by adding caged compound to the parent-peptide dilution series and demonstrate the lack of antagonist by the caged compound. Data were normalized to the maximal responses produced by the endogenous peptide agonists and are expressed as the mean ± SEM.

(D) As in C, but showing the dose-response curves for Dyn-8 (black squares), CYD8 (green triangles), and Dyn-8 in 100 nM CYD8 (open squares) at kappa (left) and mu (right) opioid receptors.

leaving the limits of neuropeptide signaling in the brain undefined.

In order to overcome these technical limitations and gain insight into the spatiotemporal dynamics of peptidergic signaling, we have developed a strategy to produce photoactivatable neuropeptides that can be applied to brain tissue at high concentrations in an inert form. These molecules can be rapidly photolyzed to trigger release of the endogenous neuropeptide with high temporal and spatial precision (Ellis-Davies, 2007). Our initial efforts focus on opioid neuropeptides, since these short peptides and their receptors are known to regulate pain sensation (Scherrer et al., 2009), behavioral reinforcement (Le Merrer et al., 2009), and addiction (Gerrits et al., 2003). Opioid peptides and their receptors are prominent in many brain regions, including hippocampus, cerebellum, striatum, amygdala, and the locus coeruleus (Khachaturian et al., 1985; Mansour et al., 1994). The opioid receptor family consists of three classically recognized receptors: mu, delta, and kappa. These are activated with differential affinity by the endogenous opioid peptides enkephalin and dynorphin, and all couple to $G\alpha_{i/o}$ such that their activation typically inhibits electrical excitability and neurotransmitter release via the opening of K^+ channels and inhibition of voltage-gated calcium channels (Wagner and Chavkin, 1995).

To enable rapid, spatially delimited delivery of opioid peptides in neural tissue, we have developed "caged" LE and Dyn-8 peptides that can be released by exposure to UV light. These peptide analogs contain a photolabile chemical moiety in a position that attenuates activity at opioid receptors. Exposure to light causes the blocking group to detach, thereby releasing the peptide agonists. As photolysis occurs with microsecond kinetics, release can be initiated on the timescale of neurotransmission. Importantly, the concentration and spatial extent of released peptide can be regulated by varying laser power and the area of illumination. We characterized these tools in brain slices and used them to define the spatiotemporal dynamics of opioid signaling with unprecedented resolution.

RESULTS

Design of Photoactivatable Opioid Neuropeptides

Enkephalins and dynorphins are the most prominent opioid peptides in the brain (Khachaturian et al., 1985). We chose to work with LE and Dyn-8 (Figure 1A) because they are the smallest and most chemically stable endogenous opioids from these peptide families. LE activates delta and mu opioid receptors with nanomolar affinity but is inactive at kappa receptors (Toll et al., 1998). The three additional C-terminal amino acids found in Dyn-8 confer nanomolar potency at kappa receptors in addition to mu and delta receptors (Toll et al., 1998). To render these peptides inactive until exposed to light, we produced analogs modified at the N-terminal tyrosine side chain with the carboxynitrobenzyl (CNB) chromophore, which photoreleases tyrosine with high quantum yield (~0.3) (Sreekumar et al., 1998) on the microsecond timescale (Tatsu et al., 1996) (see Supplemental Information, available online, for information on peptide production and handling). Extensive studies into the structure-activity relationships of enkephalins (Morley, 1980) and dynorphins (Chavkin and Goldstein, 1981) have revealed an essential role for their common N-terminal tyrosine (Y) in receptor activation. In particular, alkylation (Beddell et al., 1977) or removal (Terenius et al., 1976) of the phenolic OH group reduces the potency of enkephalin analogs, suggesting that modification of the tyrosine

side chain of LE and Dyn-8 may be a viable caging strategy. Based on these considerations, we designed CNB-Y-[Leu^5]-enkephalin (CYLE) and CNB-Y-Dyn-8 (CYD8) (Figure 1A) to release LE and Dyn-8, respectively, in response to illumination with UV light. The chemical structure of CYLE is shown in Figure 1B. Reverse-phase high-pressure liquid chromatography experiments confirmed that both peptides cleanly photorelease their parent peptides in pH 7.4 phosphate-buffered saline in response to 355 nm laser illumination (Figure S1) and that they are stable in the dark at room temperature for >48 hr (data not shown).

Activity of CYLE and CYD8 at Opioid Receptors

To determine whether CYLE and CYD8 are inactive at opioid receptors prior to photolysis, we compared their activity on opioid receptors relative to that of LE and Dyn-8, respectively, using an in vitro functional cellular assay. To detect opioid receptor activation, we utilized HEK293 cells that stably express a $G\alpha_s$-$G\alpha_i$ chimera (S.D. Liberles and L.B. Buck, personal communication). This chimeric protein allows GPCRs that normally do not signal through $G\alpha_s$ to stimulate adenylate cyclase and control the transcription of a cAMP-dependent reporter construct. Cells were cotransfected with the opioid receptor of interest and the reporter construct such that receptor activation leads to production of secreted alkaline phosphatase (SEAP). The amount of SEAP that accumulates in the media is assayed on a fluorescence plate reader with the fluorogenic substrate 4-methylumbelliferone phosphate (Liberles and Buck, 2006).

Using this assay, we obtained dose-response curves for CYLE and CYD8 at mu, delta, and kappa opioid receptors and compared those to the actions of the parent peptides (Figures 1C, 1D, and S2). The potency of CYLE was reduced 100- to 500-fold with respect to LE at both delta (LE EC_{50}, 3.2 ± 0.8 nM; CYLE EC_{50}, 1.7 ± 0.4 μM) and mu receptors [LE EC_{50}, 90 ± 11 nM; CYLE EC_{50}, 16 ± 1.7 μM (Figure 1D)]. Similar to LE, CYLE did not activate kappa receptors (Figure S2), and the presence of 100 nM CYLE did not reduce the affinity of LE at mu and delta receptors (Figure 1C) or that of Dyn-17 at kappa receptors (Figure S2), indicating that CYLE does not act as an antagonist. CYD8 exhibited similar reductions in potency in comparison to Dyn-8 at kappa (Dyn-8 EC_{50}, 7.1 ± 0.8 nM; CYD8 EC_{50}, 16 ± 1.7 μM), mu [Dyn-8 EC_{50}, 63 ± 4.4 nM; CYD8 EC_{50}, 23 ± 2.6 μM (Figure 1D)], and delta receptors [Dyn-8 EC_{50}, 9.6 ± 2.3 nM; CYD8 EC_{50}, 3.9 ± 0.6 μM (Figure S2)], with no indications of antagonism. Summary dose-response data are tabulated in Table S1. These data reveal that CYLE and CYD8 possess no significant agonist or antagonist activity at concentrations that should strongly activate receptors following photolysis.

Photorelease of Opioids in Brain Slices

In order to characterize the ability of these molecules to activate neuropeptide receptors in brain slices with spatiotemporal precision, we took advantage of the well-described opioid-receptor-mediated activation of K^+ channels in neurons of the locus coeruleus (LC). The LC is heavily innervated by enkephalinergic afferents (Curtis et al., 2001; Drolet et al., 1992), and LC neurons express a high density of mu opioid receptors in their somata and dendrites (Van Bockstaele et al., 1996a, 1996b), activation of which pauses spontaneous firing (Pepper and Henderson, 1980) by producing large outward currents (Travagli et al., 1995, 1996; Williams et al., 1982), at least in part through G protein-coupled inward rectifier K^+ (GIRK) channels.

We obtained whole-cell recordings from neurons in acute horizontal slices of rat LC (Figure 2A) and characterized the ability of CYLE to photoactivate mu receptors by releasing LE. In current-clamp recordings, these cells spontaneously fired action potentials at 2–8 Hz, while local perfusion of 10 μM LE caused a strong hyperpolarization and transient pause in spiking (Figure 2B), consistent with previous studies (Williams et al., 1982).

In voltage-clamp recordings at a holding potential of −55mV, application of 10 μM LE via a perfusion pipette placed near the cell of interest evoked average (n = 6) outward currents of 199 ± 23 pA in amplitude (Figure 2C). In contrast, when applied to the same cells, 10 μM CYLE evoked an average outward current of 5.6 ± 4 pA, measured 3.5–4 min after addition to the circulating artificial cerebrospinal fluid (ACSF) (Figure 2C). A subsequent uncaging stimulus consisting of a 5 ms flash from a 124-μm-diameter beam of 355 nm light induced a large outward current that was blocked by the addition of 2 μM naloxone (Nal), a broad-spectrum opioid receptor antagonist (Figure 2D). Additionally, photolysis of an isomer of CYLE in which the amino acid sequence was scrambled to render it inactive at opioid receptors did not produce currents (Figure S3).

To evaluate the extent and kinetics of photoactivation, we compared responses (n = 6) evoked by local application of 10 μM LE and a subsequent UV light flash in the presence of 10 μM CYLE (Figure 2E). This analysis revealed that photorelease of LE produces currents similar in amplitude to those evoked by the same concentration of locally applied LE (peak current = 207 ± 19 pA versus 179 ± 9 pA for local perfusion and photolysis, respectively) (Figure 2F). Nevertheless, consistent with rapid delivery of LE directly to the recorded cell, the onset kinetics of the light-evoked response were nearly two orders of magnitude faster than for local perfusion (τ_{on} = 349 ± 26 ms versus 11.64 ± 2.22 s for photolysis and local perfusion, respectively) (Figure 2F), such that the peak current was reached within 1–2 s after the light flash. In contrast, the kinetics of deactivation for the uncaging response were only ~2-fold faster (τ_{off} = 24 ± 2 s versus 14 ± 1 s for local perfusion and photolysis, respectively) (Figure 2F). Additionally, the responses to 15 uncaging stimuli delivered to the same cell once every 3 min were stable (Figure 2G). Thus, CYLE enables rapid and robust delivery of enkephalin in brain slices.

One advantage of caged compounds is the ability to photorelease molecules in a graded or analog fashion by varying the amount of photolysis light. This can be readily achieved by manipulating the light intensity or the area of illumination. To explore the former approach, we applied 5 ms flashes of a focused, 30-μm-diameter spot of UV light to the soma during voltage-clamp recordings and varied the light intensity. Under these conditions, the light-evoked currents in individual cells increased in amplitude with light power (Figure 3A) such that the average (n = 8) peak currents ranged from 31 ± 3 pA at 1 mW to 300 ± 32 pA at 91 mW.

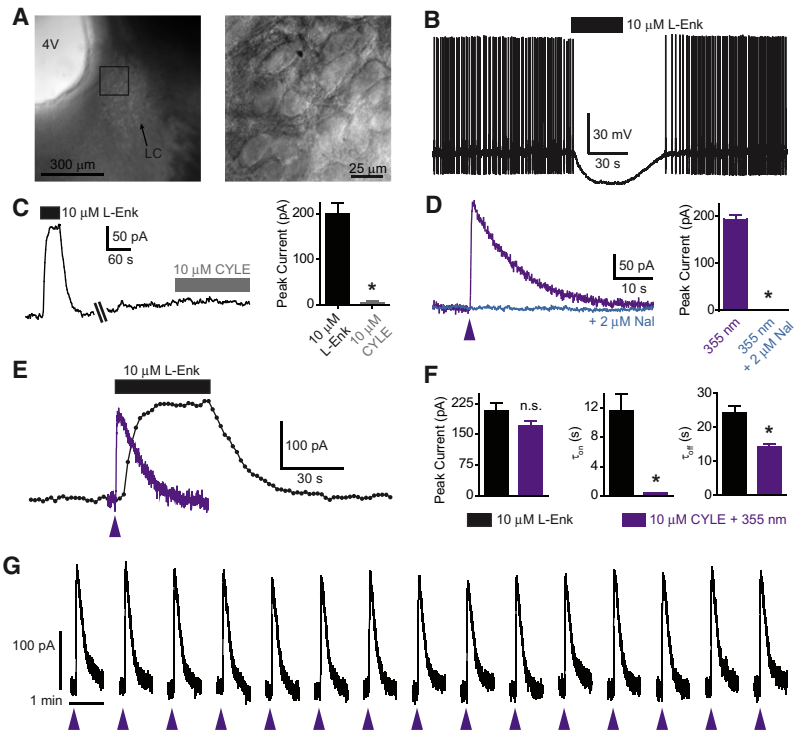

Figure 2. Rapid Activation of Outward Currents in Neurons of LC in an Acute Brain Slice by Photorelease of LE

(A) Left: Dodt contrast image of an acute horizontal brainstem slice that contains the LC. The 4th ventricle is marked (4V). Right: magnified image of the boxed region in the left image.

(B) Silencing of spontaneous action potentials in a LC neuron by local perfusion of LE.

(C) Left: outward currents in an LC neuron, resulting from application of LE (black bar) and CYLE (gray bar). Right: average peak amplitudes of currents triggered by LE (black) and CYLE (gray) (n = 6 cells). Data are expressed as the mean ± SEM. Asterisk denotes a significant difference from local perfusion of 10 μM LE ($p < 0.05$).

(D) Left: outward current in an LC neuron bathed in 10 μM CYLE evoked by a 5 ms flash of UV light in the absence (purple) or presence (blue) of the opioid antagonist Naloxone (Nal). The uncaging stimulus was applied at the time indicated by the arrowhead. Right: average peak amplitudes of UV-light-evoked currents in each condition (n = 3 cells). Asterisk denotes a significant difference from photolysis in the absence of Naloxone ($p < 0.05$).

(E) Overlay of currents from an LC neuron in response to local application of LE (black) and to an uncaging stimulus (purple) in the presence of 10 μM CYLE. The local perfusion experiment was sampled at 0.5 Hz. Each data point represents the average current during a 1 s acquisition.

(F) Average peak amplitudes (left), τ_{on} (middle), and τ_{off} (right) of currents evoked by local application of 10 μM LE (black) or an uncaging stimulus in the presence of 10 μM CYLE (purple, n = 6 cells). Asterisk denotes a significant difference from local perfusion of 10 μM LE ($p < 0.05$).

(G) Individual baseline-normalized responses from 15 uncaging stimuli applied every 3 min to the same cell. The time between episodes is omitted for clarity.

Another approach to analog delivery is to vary the area of illumination. This was achieved by shaping a collimated beam of fixed power density with a field diaphragm placed in the laser path at a location conjugate with the image plane. The area of the field of illumination was varied from 250 μm^2, which is smaller than a typical LC cell body, to 12 × 10^3 μm^2, which covers the soma and a large region of the proximal dendrites (Figure 3B). Responses were measured in both voltage- and current-clamp (Figure 3C). In voltage-clamp, varying the area of illumination produced light-evoked outward currents of various magnitude (peak current = 178 ± 29 pA versus 18 ± 6 pA for 12 × 10^3 μm^2 and 250 μm^2 fields, respectively) and duration. In current clamp, the same uncaging stimuli produced pauses in spontaneous firing of graded duration (t = 29 ± 5 s versus 4 ± 0.3 s for 12 × 10^3 μm^2 and 250 μm^2 fields, respectively) and hyperpolarizations of graded amplitude. In individual cells and across cells, the responses to each photolysis condition in both recording configurations were tightly correlated (Figure 3D). Furthermore, the onset kinetics of the light-evoked currents did not vary across the different uncaging stimuli (τ_{on} = 349 ± 26 ms versus 400 ± 66 ms versus 417 ± 112 ms for 12 × 10^3 μm^2, 4.2 × 10^3 μm^2, and 1.2 × 10^3 μm^2 fields, respectively; one-way ANOVA p = 0.81; kinetics could not be reliably measured for responses to the 250 μm^2 uncaging stimulus). These results indicate that photolysis delivers LE directly to the site of action over a range of areas.

The Ionic Basis of Enkephalin-Evoked Outward Currents

The ability to tightly regulate the area over which LE is applied provides an opportunity to study the ionic conductances that underlie the mu opioid response in LC with unprecedented accuracy. Although it has been clearly demonstrated that mu opioid receptor activation opens GIRK channels in LC neurons (Torrecilla et al., 2002), reversal potentials determined for the evoked currents in brain slices are frequently much more negative (−140mV to −120mV) than predicted for a pure K^+ conductance according to the Nernst equation (∼−105mV, typically). This observation might be accounted for by the inability to voltage-clamp currents generated in the large (Shipley et al., 1996), gap-junction-coupled dendrites (Ishimatsu and Williams, 1996; Travagli et al., 1995) of LC neurons. Several studies suggest that inhibition of a standing, voltage-insensitive Na^+ current may contribute 50% of the observed outward current response to enkephalin (Alreja and Aghajanian, 1993, 1994). Thus, the complete ionic nature of the enkephalin-evoked outward currents has been a subject of debate (Alreja and Aghajanian, 1993, 1994; Osborne and Williams, 1996; Torrecilla et al., 2002; Travagli et al., 1995).

To address this issue, we measured the reversal potential of the LE evoked outward current while restricting the uncaging area to the soma and proximal dendrites where voltage clamp is expected to be optimal (Williams and Mitchell, 2008). Importantly, the responses to the uncaging stimuli shown in Figure 3B

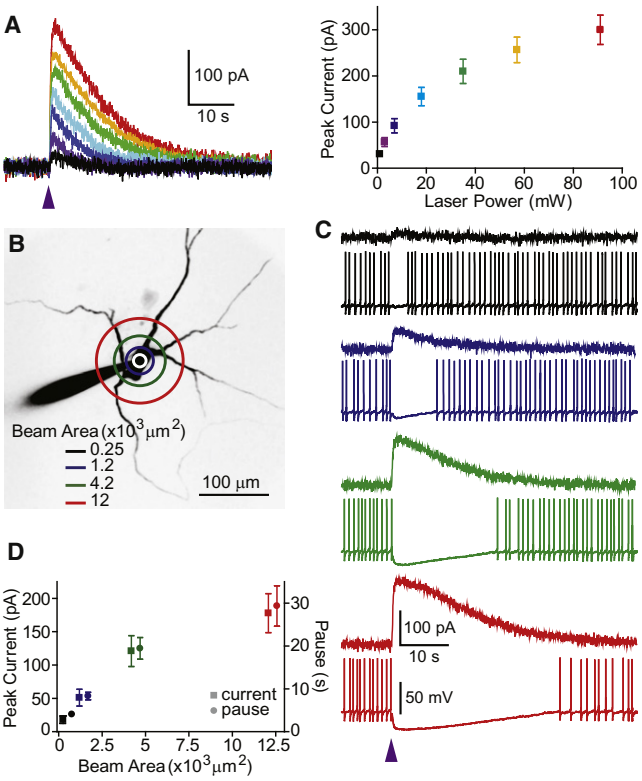

Figure 3. Graded Activation of Outward Currents in LC Neurons Evoked by Photorelease of LE

(A) Left: currents measured in an LC neuron in response to uncaging stimuli using a 30 μm spot of light focused on the soma at powers ranging from 1 (black) to 91 mW (red). Right: average peak amplitudes of currents evoked at different laser powers (n = 6 cells). Data are expressed as the mean ± SEM.

(B) Reverse-contrast two-photon laser scanning microscopy image of an LC neuron filled with Alexa Fluor-594. The colored rings and corresponding legend indicate the various diameters of a collimated photolysis beam.

(C) Current (top) and voltage (bottom) responses of an LC neuron evoked by uncaging over the areas depicted in (B).

(D) Average peak current amplitude (left axis, squares) and action-potential pause duration (right axis, circles) as a function of uncaging spot diameter. Circles are offset slightly to the right for clarity.

were not significantly attenuated by the gap junction inhibitor carbenoxolone (Figure S4), suggesting that gap junctions do not contribute to the LE-mediated currents evoked by uncaging CYLE around the soma. To measure reversal potentials in the voltage range of a K^+ conductance, we held cells at −55mV and applied negative voltage ramps to −140mV over 500 ms during the peak of the outward current (Figure 4A). A response to the ramp alone is presented with a response to the ramp after an uncaging stimulus corresponding to the 4.2 × 10^3 μm^2 beam (the green ring in Figure 2B) in Figure 4B. The average (n = 12) LE-evoked current (Figure 4C, black trace) was isolated by subtracting the baseline from the light-evoked response. After correction for the junction potential, this current reversed at −107.2mV ± 1.8mV (Figure 4D), closely matching the calculated K^+ reversal potential of −106mV ($[K^+]_{out}$ = 2.5 mM, ($[K^+]_{in}$ = 145 mM). In the presence of 3.5 mM $BaCl_2$, a GIRK channel blocker, the outward current was largely attenuated and only a small response remained (peak current = 142 ± 17 pA versus 29 ± 4 for control and 3.5 mM $BaCl_2$, respectively). The average (n = 13) LE-evoked, Ba^{2+}-insensitive current (Figures 4C and D), appeared to reverse near −140mV. We were unable to block or occlude this residual outward current with the voltage-sensitive Na^+ channel blocker tetrodotoxin (TTX), the voltage-gated K^+ channel blocker 4-AP, the voltage-gated Ca^{2+} channel blocker Cd^{2+}, or the hyperpolarization-activated cyclic-nucleotide-gated channel blocker ZD7288 and it persisted in K^+-free, Cs^+-based internal (data not shown). Thus, at least 80% of the outward current evoked by LE at the soma and proximal dendrites is carried by a Ba^{2+}-sensitive K^+ current.

The finding that somatodendritically evoked currents reverse in the predicted range for a K^+ conductance suggests that dendritic currents may indeed account for the negatively shifted reversal potentials previously obtained with bath-applied enkephalin. Therefore, using a focused, 30 μm uncaging spot, we compared the reversal potential of currents evoked by uncaging on the soma and ~150–200 μm away on a dendritic branch. Because the dendritic current was typically much smaller than the somatic current evoked by a given uncaging stimulus, we also measured the somatic current after reducing laser power to produce a response of similar amplitude. As shown for a representative cell in Figure 4E, whereas somatically evoked currents of different amplitude reverse at the same membrane potential, the reversal potential of the dendritically evoked current is shifted to more negative values. In two of five cells, the reversal potential was shifted by −12mV and −16mV, but evoked currents in the other three cells did not reverse even at −140mV, the most negative potential reached in our ramps. For quantification purposes, these were assigned a reversal potential of −140mV. By this measure, the average (n = 5) large somatic currents (182.4 ± 8.5 pA), small somatic currents (63.4 ± 5.9 pA), and dendritic currents (59.6 ± 4.3 pA; p = 0.71, paired two-tailed t test between small somatic and dendritic currents) reversed, respectively, at −110.4mV ± 1.9mV, −109.2mV ± 1.6mV, and −132.2mV ± 4.8mV ($p < 0.05$, paired two-tailed t test between small somatic and dendritic currents). Thus, opioid-activated currents in the dendrites of LC neurons cannot be reversed by somatic voltage clamp in the membrane potential range expected for K^+ currents.

Proteolytic Contribution to Enkephalin Clearance in LC

Although neuropeptides are generally thought to be degraded by extracellular proteases, the extent to which this clearance mechanism limits the duration of peptide signaling after release is unknown. To determine the contribution of peptide degradation via proteolysis to the termination of enkephalin signaling, we repeated the voltage-clamp experiment shown in Figure 3B and compared the currents evoked by light before and after the addition of the peptidase inhibitors bestatin and thiorphan (Figure 5A). This inhibitor combination blocks the degradation of enkephalin in brain tissue by >95% and increases the EC_{50} of bath-applied [Met^5]-enkephalin by 7-fold in LC (Williams et al., 1987). When the uncaging beam was restricted to the

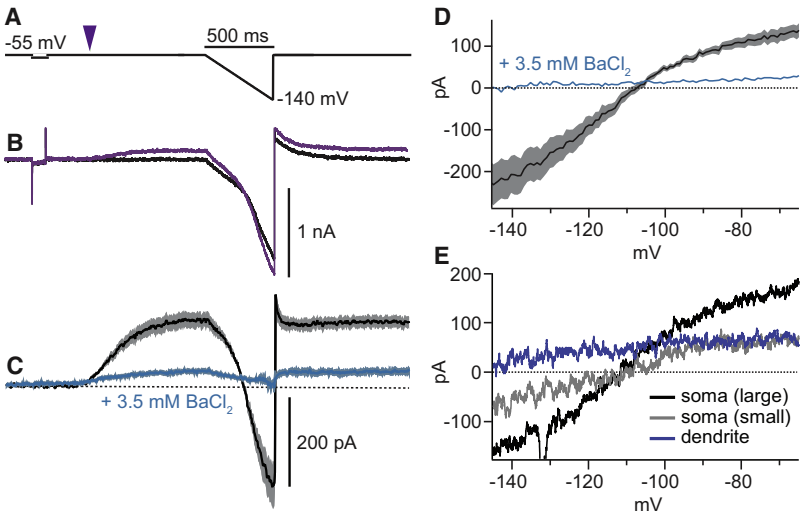

Figure 4. Activation of K^+ Currents by LE

(A) Voltage-ramp protocol for measuring K^+ currents.

(B) Currents from an LC neuron in response to the voltage-ramp protocol in the absence (black) and presence of an uncaging stimulus (purple).

(C) Average isolated responses to the uncaging stimulus and voltage ramp in the absence (black, n = 12 cells) and presence (blue, n = 13 cells) of the GIRK blocker $BaCl_2$. The dotted line indicates the baseline current in the absence of LE signaling. Average traces are shown as the mean (line) ± SEM (shaded regions).

(D) Average current-versus-voltage plot for the average currents shown in (C) indicate that the reversal potential corresponds to the calculated reversal potential of K^+.

(E) Current-versus-voltage plot for the currents generated by the indicated uncaging stimuli in an individual LC neuron.

soma (250 μm^2 and 1.2 × 10^3 μm^2 beam areas), no significant differences were observed in the peak current, charge transfer, or the time at which half of the total charge transfer occurs (TQ50%) (Figure 5B). This indicates that when opioids are released with spatial heterogeneity, the local response is determined by the local time course of peptide release and diffusion, without contribution of peptidase-mediated degradation. However, with larger uncaging areas, peptidase inhibition significantly enhanced all of these parameters. The total charge transfer at the largest area examined was particularly sensitive to this manipulation, as it was enhanced 1.8-fold, while the TQ50% was enhanced 1.6-fold. The TQ50% was used to quantify the deactivation time course, because the decay kinetics in peptidase inhibitors were not well fit by a monoexponential, as expected from the complex kinetics of buffered-diffusion reactions. These results indicate that peptidases limit the spread of enkephalin signaling when released in large volumes but that diffusion plays a larger role in limiting the spread from spatially confined release sites.

Spatial Extent of Enkephalin Signaling in LC

To determine the spatial precision with which LE can signal in LC, we focused the photolysis beam down to a nominal spot of ~2 μm in diameter and measured the current responses as the uncaging stimulus was applied at various distances along a straight line from the cell body. Due to strong scattering of UV photons by brain tissue, the effective illumination spot will be larger (Sarkisov and Wang, 2007). Laser power was adjusted to elicit a response of ~100 pA upon photolysis at the soma. Although care was taken to choose a trajectory that avoided major dendritic branches, due to the somewhat radial nature of the dendrites in the x-y plane, dendritic processes were typically present near the uncaging stimulus and most likely contributed to the measured responses. Nonetheless, the flash-evoked current amplitudes decreased with distance from the soma (Figure 6A), yielding a half-maximal response at a distance of ~100 μm. The activation kinetics of the evoked currents similarly decreased with distance from the soma (τ_{on} = 0.31 ± 0.01 s versus 0.89 ± 0.14 s for photolysis at the soma and at a distance

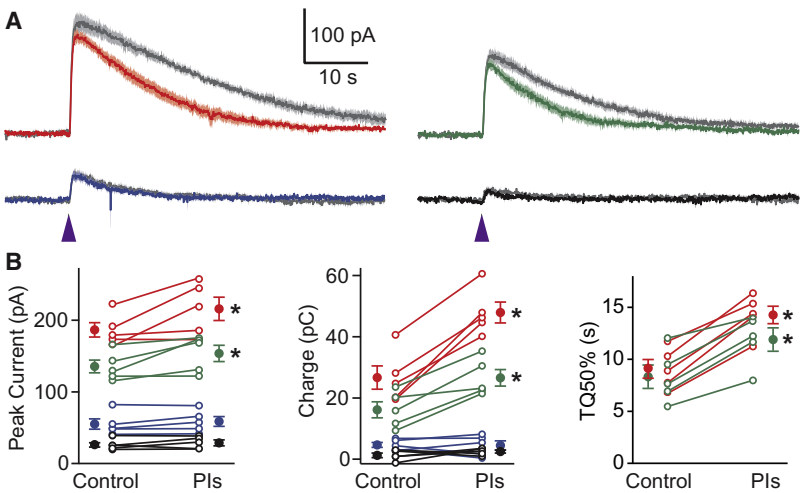

Figure 5. Effect of Peptidase Inhibitors on Light-Evoked Currents

(A) Average (n = 5 cells) responses to the uncaging stimuli before (colors) and after (gray) addition of the peptidase inhibitors. The control-condition traces are color-coded to indicate the uncaging beam area as in Figures 3B–3D. Average traces are shown as the mean (line) ± SEM (shaded regions).

(B) Peak amplitude (left), total charge transfer (middle), and time to 50% charge transfer (TQ50%, right) of the responses evoked by the uncaging stimuli for each cell in basal control conditions and after addition of peptidase inhibitors (PIs). The average population data are also shown (solid circles) as the mean ± SEM. Asterisk denotes a significant difference from control ($p < 0.05$). The small currents generated in response to the two smallest uncaging stimuli did not allow reliable calculation of TQ50%.

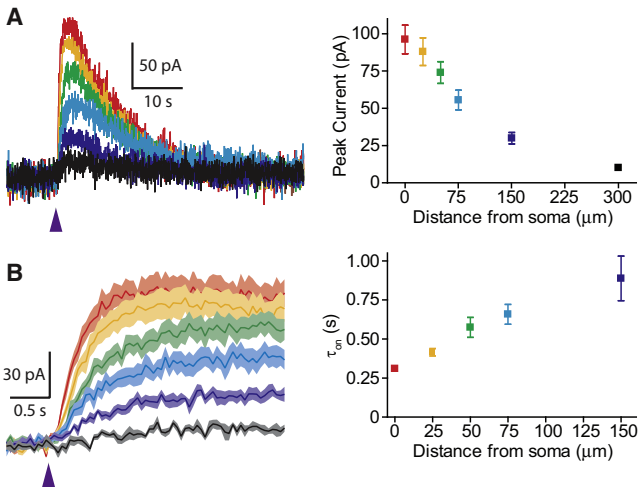

Figure 6. Spatial Extent of LE Signaling

(A) Left: currents in an LC neuron evoked by a focused 2 μm spot of UV light at various distances from the soma. Right: the average peak amplitudes (n = 9 cells) of evoked currents as a function of distance from the soma. Data are expressed as the mean ± SEM.

(B) Rising phases of the average currents (left) and quantification of the time constants of activation (τ_{on}, right) (n = 9 cells), showing faster activation kinetics for stimuli delivered near the soma.

of 150 μm, respectively; Figure 6B). Kinetic parameters could not be derived from the small individual responses to the uncaging stimulus at a distance of 300 μm and were thus excluded from this analysis. To determine whether the observed profile depends on the shape of the uncaging stimulus (in this case a cone of light focused to a 2-μm-diameter spot), we repeated this experiment using a collimated beam of 10 μm in diameter and adjusted the light intensity to again produce a response of ~100 pA at the soma. As shown in Figure S4, the spatial profiles for the elicited currents are superimposable, suggesting that the spatial extent of signaling observed reflects the spread of enkephalin signaling and is not a consequence of the optical configuration used for uncaging.

DISCUSSION

Neuropeptides are an important class of neurotransmitters that has received relatively little attention in comparison to other neuromodulators such as acetylcholine and the monoamines. Because it has been difficult to selectively stimulate neuropeptide release from distinct cell types (however, see Ludwig and Leng [2006]), our understanding of neuropeptide signaling dynamics is limited. Photoactivatable molecules enable spatiotemporally precise delivery of endogenously occurring ligands in relatively intact brain-tissue preparations. We were able to generate photoactivatable opioid neuropeptides that are sufficiently inert to allow large responses to be generated with a brief uncaging stimulus. The caged LE analog CYLE provided robust, rapid, and graded delivery of LE in acute brain slices. The ability to spatially restrict release allowed us to selectively evoke currents from regions of neurons that can be effectively voltage clamped in order to accurately measure the reversal potential of the mu-opioid-receptor-mediated K^+ current, which was not previously possible in brain slices of LC. These features further enabled us to quantitatively characterize the mechanisms governing peptide clearance and delineate the spatial profile of enkephalinergic volume transmission for the first time.

Based on extensive prior pharmacology, we identified the N-terminal tyrosine side chain as a caging site where the relatively small CNB chromophore sufficiently attenuates potency on both LE and Dyn-8. Peptides may be inherently more difficult to "cage" than small molecules, as the caging group will only interfere with one of multiple interaction sites with receptors. In particular, hydrophobic interactions contribute greatly to peptide-receptor binding, and hydrophobic side chains lack functional handles for attaching caging groups. For these reasons, the full-length Dyn-17 or beta-endorphin may be more difficult to cage by the same approach.

CNB-tyrosine photolysis occurs with microsecond kinetics following a light flash (Sreekumar et al., 1998; Tatsu et al., 1996). Thus, the time course of activation we observed in slices likely reflects the time required for ligand binding and engagement of the G protein-mediated signaling pathway that activates GIRK channels. Indeed, we observed a 50–100 ms delay from the flash to the current onset and a peak response within 1–2 s, which closely matches the rates observed for $GABA_B$R-mediated GIRK activation in dissociated cells using rapid perfusion techniques (Ingram et al., 1997; Sodickson and Bean, 1996). However, the offset kinetics we observed are orders of magnitude slower than those measured in dissociated cells, where currents cease within 1–2 s of agonist washout. Instead, photorelease produced deactivation kinetics that were only 2-fold faster than those obtained with local perfusion, likely reflecting slow diffusion of released peptide away from the recorded cell in neural tissue and concomitant proteolytic cleavage. Indeed, addition of a protease inhibitor cocktail slowed deactivation of the response to photolysis over large areas.

Prompted by the ability to spatially confine LE release, we revisited previous studies into opioid actions on rat LC neurons that were unable to unambiguously identify a K^+ current using reversal potential measurements in brain slices (Osborne and Williams, 1996; Travagli et al., 1995). The reversal potential of the LE-dependent current that we measured is accounted for by a pure K^+ current and 80% of the outward current was blocked by a high concentration of Ba^{2+}, consistent with a dominant role of GIRKs. It has also been proposed that downregulation of a cAMP-dependent standing Na^+ current contributes 50% of the opioid response in rat LC (Alreja and Aghajanian, 1993, 1994). Although we cannot rule out that this component mediates the remaining 20% of the current not sensitive to Ba^{2+} or that this Na^+-permeable channel may be enriched in the dendritic regions not activated by the somatodendritically restricted uncaging stimulus, our results clearly demonstrate that the majority of the current in the soma and proximal portions of the dendrites is carried by K^+ channels and thus cannot reflect the closing of Na^+ channels. Consistent with previous work that suggests that poor voltage clamp of K^+ currents originating in LC dendrites may underlie the apparent negative shift in K^+ reversal potential (Ishimatsu and Williams, 1996; Travagli et al., 1995),

photorelease of LE in the distal dendrites evoked currents that reversed at membrane potentials much more negative than somatically evoked currents. This shifted membrane potential can arise from poor space clamp of the large LC dendrites, K^+ currents activated in unclamped and gap-junction-coupled neighboring cells, or from other dendritically localized and opioid modulated conductances.

By varying the laser power and uncaging area used to photorelease LE, we found a correlation between the amplitude and duration of the outward current in voltage clamp and the duration of the pause in spontaneous firing recorded in current clamp (Figure 3). The responses to the smallest stimuli demonstrate that small outward currents near the detection limit are sufficient to prevent just a few action potentials without causing significant hyperpolarization. At the opposite extreme, strong uncaging causes a large somatic hyperpolarization and pauses action potential firing for 30 s or longer. Thus, the effect of enkephalin on LC firing can be subtle or dramatic, highlighting that neuropeptides are capable of temporally precise actions in addition to slow volume transmission.

We found that LE could generate opioid-receptor-mediated currents when released ~150 μm from the recorded cell. The slower-onset kinetics observed when LE was released at locations distant from the soma suggest that the photolyzed peptide diffused from the release site to activate receptors on the soma and proximal dendrites. These distances are large compared to those over which fast-acting neurotransmitters such as glutamate (Carter et al., 2007) and GABA (Chalifoux and Carter, 2011) can spread, as clearance mechanisms for these neurotransmitters are present at high density in neural tissue. Under the conditions of our experiments, LE was nearly inactive when released 300 μm from the soma, which reflects the limit of detection by mu opioid receptors due to dilution of the peptide as it diffuses away from the release site. Assuming a diffusion-limited process, this absolute boundary depends not only on the initial quantity released, but also on the affinity of the receptor for the ligand. Our results may overestimate the mobility of LE in LC due to activation of receptors on dendrites that are closer to the release site than the soma and contributions from currents originating in gap-junction-coupled neurons. Nonetheless, our results indicate that enkephalin can effectively function as a volume transmitter in LC and define the spatial profile of the spread of enkephalinergic signaling from a single release site. The spatial profile of signaling may be different in other brain regions due to variations in the densities and identities of proteases and possible differences in diffusional mobility.

Although we obtained similar results using two differently shaped photolysis beams, UV light scatters extensively in brain tissue. Studies in which similar spot sizes (10–25 μm) were employed for UV uncaging of glutamate in brain slices report 25–50 μm lateral resolution (Katz and Dalva, 1994; Kim and Kandler, 2003). Below the surface of the brain slice, light scattering enlarges the photolysis spot by approximately 2-fold in the x-y dimensions (Sarkisov and Wang, 2007), consistent with these observations. Because one-photon uncaging provides poor spatial control in the z-dimension, it is most practical to consider our results in terms of area of photolysis in the plane of the recorded cell. Thus, we estimate that the 10-μm-diameter collimated uncaging stimulus illuminates an area of ~300 μm^2 at the depth of our recordings. At the light intensity employed, LE evoked substantial currents when released 150 μm from the uncaging site within 1–2 s of the light flash, indicating that the enkephalin signal rapidly spreads through at least 70,000 μm^2 of tissue, which is ~200-fold greater than the area of origin. To more accurately address peptide mobility in brain tissue, two-photon sensitive caging groups must be employed so that release will be restricted to μm^3-scale volumes.

Here, we have described photoactivatable tools for the study of opioid signaling within the mammalian brain. By caging both LE and Dyn-8, we provide reagents that can be used to study mu, delta, and kappa receptors. Using UV-mediated photolysis of caged LE in brain slices, we demonstrated that somatic mu receptors in the LC generate an outward current mediated primarily by K^+ channels. These reagents allowed us to probe the mechanisms that regulate the spread of opioid signaling in brain tissue and revealed that with graded, temporally precise, and spatially confined release, neuropeptides are capable of subtle and relatively short-lasting modulation of neuronal function. This approach represents a general strategy for probing the spatiotemporal dynamics of neuropeptides and should be applicable to other peptide transmitters.

These reagents are expected to interface well with two-photon Ca^{2+} and voltage imaging methods, as the CNB chromophore exhibits poor sensitivity to two-photon excitation. Similarly, one-photon excitation, with the visible wavelengths used to image fluorophores such as GFP and activate light-sensitive ion channels such as channelrhodopsin, is also compatible with our probes. However, the intense UV light used for uncaging can photobleach fluorophores and partially activate channelrhodopsin, so care must be taken to control the area of illumination and minimize the requisite UV light intensity in these contexts. Extension to in vivo studies, including amperometry to measure the effects of opioids on monoamine release, should be possible by equipping optrodes and fiberoptic coupled carbon fibers with perfusion lines for peptide delivery and may thus enable spatiotemporal studies into opioidergic modulation of behavior with unprecedented precision.

EXPERIMENTAL PROCEDURES

Peptide Synthesis, Purification, and Stock Preparation

Custom chemical synthesis was carried out by Peptech Corporation (Burlington, MA) using standard Fmoc-based solid-phase peptide synthesis. The carboxynitrobenzyl-modified tyrosine was prepared by modifying established protocols (Sreekumar et al., 1998). After arrival, CYLE and CYD8 were typically handled under lighting filtered using Rosculux #312 Canary optical filter paper to remove any traces of UV light that could lead to unintentional photolysis. It was essential to further purify the synthetic material by semipreparative reverse-phase high-pressure liquid chromatography (RP-HPLC, Agilent) to remove contaminating photolysis products, which typically included ~1% LE or Dyn-8. Crucially, the UV (and VIS) lamps on the detector were turned off during the purification to prevent photolysis of the purified material. Purified solid material was dissolved in 50% DMSO/water and diluted to a concentration of 10 mM. Stock concentrations were determined by UV/VIS spectroscopy using an extinction coefficient of 1,000 M^{-1} cm^{-1} at 355 nm for the carboxynitrobenzyl-modified tyrosine (Sreekumar et al., 1998).

Photolysis in Solution

A 100 μl sample of either 1 mM CYLE or CYD8 in phosphate-buffered saline, pH 7.2, contained in a quartz cuvette, was placed for 30 s in the path of a 100 KHz pulsed q-switched UV laser (DPSS, Santa Clara, Ca) producing ~800 mW of 354.7 nm light. The samples were then analyzed by RP-HPLC on a 4.6 mm × 150 mm Zorbax SB-C8 column (5 μm particle size) in H_2O, MeCN, 0.1% TFA at 1 ml/min. LE and CYLE were resolved by a gradient from 30% to 70% MeCN over 10 min. Dyn-8 and CYD8 were resolved by a gradient from 25% to 70% MeCN over 10 min. Samples were monitored at 210 nm, 280 nm, and 350 nm. Nonphotolyzed CYLE, CYD8, LE, and Dyn-8 samples were prepared and run under the same conditions. Although addition of the parent peptides to photolyzed samples increased the product peaks as expected, further analysis by mass spectrometry confirmed photolytic conversion of CYLE to LE and CYD8 to Dyn-8 (data not shown).

Cell Culture and SEAP Assay

HEK293 cells stably transfected with a chimeric G_s-G_i protein (S.D. Liberles and L.B. Buck, personal communication; Liberles and Buck, 2006) were grown in DMEM (Invitrogen) containing 5% FBS (Invitrogen) and 500 μg/ml G-418 (Invitrogen) and maintained at 37°C in an atmosphere of 5% CO_2. Cells were plated in 96-well plates at 50,000 cells/well and cotransfected with the GPCR and reporter plasmid using Lipofectamine (Invitrogen) and PLUS reagent (Invitrogen). The transfection media was replaced with ligand-containing DMEM (200 μl/well) and cells were incubated for 36–48 hr 37°C/5% CO_2. Care was taken to avoid exposure to bright, nonfiltered light. Each plate was then wrapped in plastic wrap and incubated at 68°C for 2 hr to heat-inactivate native phosphatases. After transferring 100 μl aliquots from each well to a fresh 96-well plate, 100 μl of an aqueous buffer containing 2 M diethanolamine bicarbonate and 1.2 mM methylumbelliferone phosphate, pH 10.0, was added to each well. Plates were imaged using a Perkin Elmer Envision plate reader using optical settings for methylumbelliferone fluorescence, taking care to image all conditions to be compared on the same day for a single receptor at the same time point after MUP addition. In every individual experiment, the noncaged parent ligand (LE or Dyn-8) was evaluated alongside the caged compound (CYLE or CYD8) at the same receptor and used to normalize data across trials. cDNAs encoding human delta (OPRD1) and human kappa opioid receptors (OPRK1) contained an N-terminal 3xHA epitope tag (Missouri S&T cDNA Resource center, http://www.cdna.org) and the murine mu opioid receptor (OPRM1) contained an N-terminal FLAG epitope tag. Data shown reflect the average of six replicates run in parallel for each condition.

Animal Handling and Slice Preparation

Animals were handled according to protocols that were approved by the Harvard Standing Committee on Animal Care and are in accordance with Federal guidelines. Postnatal day 22–29 Long-Evans rats were anesthetized by inhalation of isoflurane and cardiac perfused with ice-cold ACSF containing 127 mM NaCl, 2.5 mM KCl, 25 mM $NaHCO_3$, 1.25 mM NaH_2PO_4, 2.0 mM $CaCl_2$, 1.0 mM $MgCl_2$, and 25 mM glucose, equilibrated with 95% O_2/5% CO_2, osmolarity 307. Horizontal slices of locus coeruleus were prepared in a cold choline-ACSF containing 25 mM $NaHCO_3$, 1.25 mM NaH_2PO_4, 2.5 mM KCl, 7 mM $MgCl_2$, 25 mM glucose, 1 mM $CaCl_2$, 110 mM choline chloride, 11.6 mM ascorbic acid, and 3.1 mM pyruvic acid, and equilibrated with 95% O_2/5% CO_2. Slices of 260 μm thickness were cut with a Leica VT1000s (Leica Instruments, Nussloch, Germany) and transferred to a holding chamber containing ACSF. Slices were incubated at 32°C for 30–45 min and then left at room temperature (20–22°C) until recordings were performed.

Electrophysiology

All recordings were performed within 5 hr of slice cutting in a submerged slice chamber perfused with ACSF warmed to 32°C and equilibrated with 95% O_2/5% CO_2. Whole-cell recordings were made from LC neurons visualized using Dodt gradient contrast. The LC was identified in horizontal brainstem slices as a distinct, relatively translucent cluster of cells with exceptionally large somata, typically 20–30 μm in diameter. For current-clamp recordings and voltage-clamp recordings measuring K^+ currents, patch pipettes (open pipette resistance 1.6–2.2 MΩ) were filled with an internal solution containing 135 mM $KMeSO_4$, 5 mM KCl, 5 mM HEPES, 1.1 mM EGTA, 4 mM MgATP, 0.3 mM Na_2GTP, and 10 mM Na_2creatine phosphate (pH 7.25, osmolarity 286). For the experiments in Figures 4E and 6, 20 μM Alexa 594 (Molecular Probes) was included in the internal solution.

Recordings were made with an Axoclamp 200B amplifier (Axon Instruments, Union City, CA). Data were filtered at 5 kHz and sampled at 10 kHz. Cells were held at −55mV in voltage-clamp mode, and no current was injected in current-clamp mode. Cells were rejected if holding currents exceeded −200 pA. Series and input resistance were measured throughout the experiment, and recordings were discarded if series resistance exceeded 15 MΩ. Series resistance was not compensated. Liquid junction potentials of ~−8mV were not corrected except when calculating the reversal potentials in Figure 4. In these experiments, we only accepted recordings in which series resistance was between 5 and 8 MΩ and compensated for whole-cell capacitance and series resistance by 60%–80%.

Pharmacology

In all experiments, the following pharmacological agents were used in the extracellular solution at final concentrations of 10 μM CPP (Tocris), 10 μM NBQX (Tocris), and 25 μM picrotoxin (Tocris). In some experiments, additional agents were added, as indicated in the text: 2 μM naloxone (Tocris), 100 μM carbenoxolone (Tocris), 3 μM thiorphan (Sigma), 20 μM bestatin (Sigma), 3.5 mM $BaCl_2$ (Sigma), 1 μM TTX (Tocris), 1 mM 4-AP (Tocris), 300 μM $CdCl_2$ (Sigma), and 50 μM ZD7288 (Tocris).

UV Uncaging

For UV uncaging, we used a custom setup based on a BX51WI microscope (Olympus). The output of a 100 KHz pulsed q-switched UV laser (Model 3501, DPSS, Santa Clara, Ca) producing ~800 mW of 354.7 nm light was launched into a multimode, 200-μm-inner-diameter optical fiber with a numerical aperture of 0.22 (OZ Optics, Ottawa, Ontario, Canada). The beam was shuttered at the laser head (OZ Optics, part number HPUC-2,A3HP-355-M-10BQ-1-SH) and collimated at the output of the fiber using either a factory- (OZ Optics, part number HPUC0-2,A3HP-355-M-25BQ) or custom-built collimator to produce a 10-mm-diameter beam. Laser pulses were controlled by opening the shutter, waiting for mechanical vibrations in the fiber launch to dampen, and then q-switching the laser on and off. Light power levels were monitored with a PDA25K amplified photodiode (Thorlabs). Uncaging areas were measured by imaging laser-evoked fluorescence from a thin layer of an aqueous fluorescein solution that was sandwiched between two glass coverslips and placed in the sample chamber.

For the experiments in Figures 2, 3B–3D, 4B–4D, and 5, the 10-mm-diameter beam was focused using a planoconvex lens onto the back focal plane of a 60× water-immersion, infinity-corrected objective with a numerical aperture of 0.90 (Olympus) to produce a collimated beam of ~124 μm in diameter. Light intensity was attenuated to ~25 mW, measured as a 10-mm-diameter beam at the back aperture of the objective with the planoconvex lens removed from the light path. An iris placed in the light path in a conjugate image plane served as a field diaphragm. The iris was adjusted such that the diameter of the area in the tissue exposed to UV light was either ~124 μm, ~73 μm, ~39 μm, or ~18 μm, corresponding to the beam areas of 12×10^3 μm^2, 4.2×10^3 μm^2, 1.2×10^3 μm^2, or 250 μm^2, respectively, as indicated in the text. For the experiments in Figures 3A and 4E, the beam was launched directly into the objective to produce a focused UV spot of ~30 μm in diameter, and power was modulated with neutral density filters to range from 1 mW to 91 mW, measured as a 10-mm-diameter beam at the back aperture of the objective. In this optical configuration, photolysis at light intensities >91 mW led to unstable recordings. For the experiments in Figure 6, the output from a multimode, 25-μm-inner-diameter optical fiber with an numerical aperture of 0.13 (OZ Optics, Ottawa, Ontario, Canada) was collimated to a 10-mm-diameter beam and launched directly into the objective to produce a focused UV spot of ~2 μm in diameter at the sample. Power was modulated empirically to yield a ~100 pA response at the soma. For the experiments in Figure S4, the output from the 25 μm fiber was collimated to a 2.5-mm-diameter beam that was focused using a planoconvex lens onto the back focal plane of the objective. The field diaphragm was adjusted to produce a collimated beam of 10 μm in diameter at the sample.

Two-Photon Imaging

Neurons in acute slices were loaded with 100 μm Alexa Fluor 594 via a patch pipette, and images were taken using a custom-built two-photon microscope and a Chameleon Ti-Sapphire laser tuned to 840 nm.

Data Analysis and Statistics

All data are expressed as the mean ± SEM. In the figures, average traces are shown as the mean (line) ± the SEM (shaded regions or bars). A two-tailed t test was used to determine significance of differences across conditions in Figures 2 and 5. $p < 0.05$ was considered significant.

SUPPLEMENTAL INFORMATION

Supplemental Information includes five figures and one table and can be found with this article online at doi:10.1016/j.neuron.2011.11.016.

ACKNOWLEDGMENTS

The authors thank members of the Sabatini laboratory and G. Pekkurnaz for helpful comments during the preparation of the manuscript. We thank S.D. Liberles, L.B. Buck, and J. Lemon for assistance with the SEAP assays and for the gift of reagents; J.L. Whistler for the mu opioid receptor plasmid DNA; J.B. Cohen and D.C. Chiara for HPLC access; J.T. Williams for insightful discussions; R. Shah for technical support; and the ICCB-Longwood screening facility for access to plate readers. The work was funded by a grant from the Helen Hay Whitney Foundation (postdoctoral fellowship) to M.R.B. and a grant from the National Institute of Mental Health (MH085498) to B.L.S. M.R.B. conducted the experiments and data analysis. M.R.B. and B.L.S. designed the experiments and wrote the manuscript.

Accepted: November 8, 2011
Published: January 25, 2012

REFERENCES

Adamantidis, A., Carter, M.C., and de Lecea, L. (2010). Optogenetic deconstruction of sleep-wake circuitry in the brain. Front. Mol. Neurosci. *2*, 31.

Alreja, M., and Aghajanian, G.K. (1993). Opiates suppress a resting sodium-dependent inward current and activate an outward potassium current in locus coeruleus neurons. J. Neurosci. *13*, 3525–3532.

Alreja, M., and Aghajanian, G.K. (1994). QX-314 blocks the potassium but not the sodium-dependent component of the opiate response in locus coeruleus neurons. Brain Res. *639*, 320–324.

Beddell, C.R., Clark, R.B., Hardy, G.W., Lowe, L.A., Ubatuba, F.B., Vane, J.R., and Wilkinson, S. (1977). Structural requirements for opioid activity of analogues of the enkephalins. Proc. R. Soc. Lond. B Biol. Sci. *198*, 249–265.

Carter, A.G., Soler-Llavina, G.J., and Sabatini, B.L. (2007). Timing and location of synaptic inputs determine modes of subthreshold integration in striatal medium spiny neurons. J. Neurosci. *27*, 8967–8977.

Chalifoux, J.R., and Carter, A.G. (2011). GABAB receptor modulation of voltage-sensitive calcium channels in spines and dendrites. J. Neurosci. *31*, 4221–4232.

Chavkin, C., and Goldstein, A. (1981). Specific receptor for the opioid peptide dynorphin: structure—activity relationships. Proc. Natl. Acad. Sci. USA *78*, 6543–6547.

Curtis, A.L., Bello, N.T., and Valentino, R.J. (2001). Evidence for functional release of endogenous opioids in the locus ceruleus during stress termination. J. Neurosci. *21*, RC152.

Drolet, G., Van Bockstaele, E.J., and Aston-Jones, G. (1992). Robust enkephalin innervation of the locus coeruleus from the rostral medulla. J. Neurosci. *12*, 3162–3174.

Duggan, A.W. (2000). Neuropeptide spread in the brain and spinal cord. Prog. Brain Res. *125*, 369–380.

Duggan, A.W., and North, R.A. (1983). Electrophysiology of opioids. Pharmacol. Rev. *35*, 219–281.

Ellis-Davies, G.C.R. (2007). Caged compounds: photorelease technology for control of cellular chemistry and physiology. Nat. Methods *4*, 619–628.

Gerrits, M.A., Lesscher, H.B., and van Ree, J.M. (2003). Drug dependence and the endogenous opioid system. Eur. Neuropsychopharmacol. *13*, 424–434.

Hökfelt, T., Broberger, C., Xu, Z.Q., Sergeyev, V., Ubink, R., and Diez, M. (2000). Neuropeptides—an overview. Neuropharmacology *39*, 1337–1356.

Ingram, S., Wilding, T.J., McCleskey, E.W., and Williams, J.T. (1997). Efficacy and kinetics of opioid action on acutely dissociated neurons. Mol. Pharmacol. *52*, 136–143.

Insel, T.R. (2010). The challenge of translation in social neuroscience: a review of oxytocin, vasopressin, and affiliative behavior. Neuron *65*, 768–779.

Ishimatsu, M., and Williams, J.T. (1996). Synchronous activity in locus coeruleus results from dendritic interactions in pericoerulear regions. J. Neurosci. *16*, 5196–5204.

Katz, L.C., and Dalva, M.B. (1994). Scanning laser photostimulation: a new approach for analyzing brain circuits. J. Neurosci. Methods *54*, 205–218.

Khachaturian, H., Lewis, M.E., Schafer, M.K.-H., and Watson, S.J. (1985). Anatomy of CNS opioid systems. Trends Neurosci. *8*, 111–119.

Kim, G., and Kandler, K. (2003). Elimination and strengthening of glycinergic/GABAergic connections during tonotopic map formation. Nat. Neurosci. *6*, 282–290.

Knoll, A.T., and Carlezon, W.A., Jr. (2010). Dynorphin, stress, and depression. Brain Res. *1314*, 56–73.

Le Merrer, J., Becker, J.A., Befort, K., and Kieffer, B.L. (2009). Reward processing by the opioid system in the brain. Physiol. Rev. *89*, 1379–1412.

Liberles, S.D., and Buck, L.B. (2006). A second class of chemosensory receptors in the olfactory epithelium. Nature *442*, 645–650.

Ludwig, M., and Leng, G. (2006). Dendritic peptide release and peptide-dependent behaviours. Nat. Rev. Neurosci. *7*, 126–136.

Lupica, C.R., Proctor, W.R., and Dunwiddie, T.V. (1992). Dissociation of mu and delta opioid receptor-mediated reductions in evoked and spontaneous synaptic inhibition in the rat hippocampus in vitro. Brain Res. *593*, 226–238.

Mansour, A., Fox, C.A., Burke, S., Meng, F., Thompson, R.C., Akil, H., and Watson, S.J. (1994). Mu, delta, and kappa opioid receptor mRNA expression in the rat CNS: an in situ hybridization study. J. Comp. Neurol. *350*, 412–438.

Morley, J.S. (1980). Structure-activity relationships of enkephalin-like peptides. Annu. Rev. Pharmacol. Toxicol. *20*, 81–110.

Morton, G.J., Cummings, D.E., Baskin, D.G., Barsh, G.S., and Schwartz, M.W. (2006). Central nervous system control of food intake and body weight. Nature *443*, 289–295.

Osborne, P.B., and Williams, J.T. (1996). Forskolin enhancement of opioid currents in rat locus coeruleus neurons. J. Neurophysiol. *76*, 1559–1565.

Pepper, C.M., and Henderson, G. (1980). Opiates and opioid peptides hyperpolarize locus coeruleus neurons in vitro. Science *209*, 394–395.

Sarkisov, D.V., and Wang, S.S.-H. (2007). Combining uncaging techniques with patch-clamp recording and optical physiology. In Patch-clamp Analysis: Advanced Techniques, W. Walz, ed. (New York: Humana Press), pp. 149–168.

Scherrer, G., Imamachi, N., Cao, Y.Q., Contet, C., Mennicken, F., O'Donnell, D., Kieffer, B.L., and Basbaum, A.I. (2009). Dissociation of the opioid receptor mechanisms that control mechanical and heat pain. Cell *137*, 1148–1159.

Shipley, M.T., Fu, L., Ennis, M., Liu, W.L., and Aston-Jones, G. (1996). Dendrites of locus coeruleus neurons extend preferentially into two pericoerulear zones. J. Comp. Neurol. *365*, 56–68.

Sodickson, D.L., and Bean, B.P. (1996). GABAB receptor-activated inwardly rectifying potassium current in dissociated hippocampal CA3 neurons. J. Neurosci. *16*, 6374–6385.

Sreekumar, R., Ikebe, M., Fay, F.S., and Walker, J.W. (1998). Biologically active peptides caged on tyrosine. Methods Enzymol. *291*, 78–94.

Strand, F.L. (1999). Neuropeptides as neurotransmitters, neuromodulators, and neurohormones. In Neuropeptides: Regulators of physiological processes, F.L. Strand, ed. (Cambridge, MA: The MIT Press).

Svoboda, K.R., Adams, C.E., and Lupica, C.R. (1999). Opioid receptor subtype expression defines morphologically distinct classes of hippocampal interneurons. J. Neurosci. *19*, 85–95.

Tallent, M.K. (2008). Presynaptic inhibition of glutamate release by neuropeptides: use-dependent synaptic modification. Results Probl. Cell Differ. *44*, 177–200.

Tatsu, Y., Shigeri, Y., Sogabe, S., Yumoto, N., and Yoshikawa, S. (1996). Solid-phase synthesis of caged peptides using tyrosine modified with a photocleavable protecting group: application to the synthesis of caged neuropeptide Y. Biochem. Biophys. Res. Commun. *227*, 688–693.

Terenius, L., Wahlström, A., Lindeberg, G., Karlsson, S., and Ragnarsson, U. (1976). Opiate receptor affinity of peptides related to Leu-enkephalin. Biochem. Biophys. Res. Commun. *71*, 175–179.

Toll, L., Berzetei-Gurske, I.P., Polgar, W.E., Brandt, S.R., Adapa, I.D., Rodriguez, L., Schwartz, R.W., Haggart, D., O'Brien, A., White, A., et al. (1998). Standard binding and functional assays related to medications development division testing for potential cocaine and opiate narcotic treatment medications. NIDA Res. Monogr. *178*, 440–466.

Torrecilla, M., Marker, C.L., Cintora, S.C., Stoffel, M., Williams, J.T., and Wickman, K. (2002). G-protein-gated potassium channels containing Kir3.2 and Kir3.3 subunits mediate the acute inhibitory effects of opioids on locus ceruleus neurons. J. Neurosci. *22*, 4328–4334.

Travagli, R.A., Dunwiddie, T.V., and Williams, J.T. (1995). Opioid inhibition in locus ceruleus. J. Neurophysiol. *74*, 519–528.

Travagli, R.A., Wessendorf, M., and Williams, J.T. (1996). Dendritic arbor of locus coeruleus neurons contributes to opioid inhibition. J. Neurophysiol. *75*, 2029–2035.

Urban, J.D., Clarke, W.P., von Zastrow, M., Nichols, D.E., Kobilka, B., Weinstein, H., Javitch, J.A., Roth, B.L., Christopoulos, A., Sexton, P.M., et al. (2007). Functional selectivity and classical concepts of quantitative pharmacology. J. Pharmacol. Exp. Ther. *320*, 1–13.

Van Bockstaele, E.J., Colago, E.E., Cheng, P., Moriwaki, A., Uhl, G.R., and Pickel, V.M. (1996a). Ultrastructural evidence for prominent distribution of the mu-opioid receptor at extrasynaptic sites on noradrenergic dendrites in the rat nucleus locus coeruleus. J. Neurosci. *16*, 5037–5048.

Van Bockstaele, E.J., Colago, E.E., Moriwaki, A., and Uhl, G.R. (1996b). Mu-opioid receptor is located on the plasma membrane of dendrites that receive asymmetric synapses from axon terminals containing leucine-enkephalin in the rat nucleus locus coeruleus. J. Comp. Neurol. *376*, 65–74.

Wagner, J.J., and Chavkin, C.I. (1995). Neuropharmacology of Endogenous Opioid Peptides. In Psychopharmacology: The Fourth Generation of Progress, F.E. Bloom and D.J. Kupfer, eds. (New York: Raven Press, Ltd.).

Williams, J.T., Christie, M.J., North, R.A., and Roques, B.P. (1987). Potentiation of enkephalin action by peptidase inhibitors in rat locus ceruleus in vitro. J. Pharmacol. Exp. Ther. *243*, 397–401.

Williams, J.T., Egan, T.M., and North, R.A. (1982). Enkephalin opens potassium channels on mammalian central neurones. Nature *299*, 74–77.

Williams, S.R., and Mitchell, S.J. (2008). Direct measurement of somatic voltage clamp errors in central neurons. Nat. Neurosci. *11*, 790–798.